IEEE Access
Multidisciplinary | Rapid Review | Open Access Journal

Received November 30, 2017, accepted January 15, 2018, date of publication February 5, 2018, date of current version April 18, 2018.

Digital Object Identifier 10.1109/ACCESS.2018.2802038

Measurements and Analysis of Large-Scale Path Loss Model at 14 and 22 GHz in Indoor Corridor

NICHOLAS O. OYIE, (Student Member, IEEE), AND THOMAS J. O. AFULLO, (Member, IEEE)
Discipline of Electrical, Electronic and Computer Engineering, University of KwaZulu-Natal, Durban 4041, South Africa
Corresponding author: Nicholas O. Oyie (217063428@stu.ukzn.ac.za)

ABSTRACT Fifth generation wireless communications will exploit the enormous chunk of bandwidth available at millimeter-wave frequency bands. Accordingly, an accurate and simple path loss model is critical for indoor environments, where deployment is likely to occur. We conducted measurement campaigns in the 14 and 22 GHz frequency bands in a typical indoor corridor environment on 5th floor of the Discipline of Electrical, Electronic and Computer Engineering building, University of KwaZulu-Natal, Howard Campus, South Africa. This paper presents details of measurement campaigns with unique transmitter-receiver combinations using a costume-designed channel sounder. The acquired measurement results provide large-scale path loss statistics in an open-plan indoor environment in line-of-sight and non-line-of-sight conditions. An effective application of dual slope single-frequency directional large-scale path loss model is evaluated based on the acquired measurement data. The application of dual slope large-scale path loss model is supported by a comprehensive analysis and consideration of propagation mechanisms, such as reflection and diffraction resulting in modal attenuation. Validated results show that dual slope large-scale path loss model applied in this paper outperforms close-in reference distance model that assumes the impact of propagating wave guiding effect in indoor corridors.

INDEX TERMS 5G, channel sounder, indoor corridor measurements, millimeter-wave propagation, path loss modeling.

I. INTRODUCTION

The limitation of bandwidth has often constrained today's cellular communication providers' pursuit to provide high quality contents on wireless devices through mobile broadband networks. This limitation is occasioned by current global communication systems that support only the frequency bands between 700 MHz and 2.6 GHz [1]–[3]. Millimeter-wave (mmWave) frequency bands avail massive chunk of bandwidth and motivate invention of future communication systems. Certainly, mmWave frequency range will play a crucial role in 5G wireless communications [4]. Therefore, application of frequency bands beyond the microwave band (usually 3 GHz band) is anticipated. Super high frequency (SHF) band (3–30 GHz spectrum) and extremely high frequency (EHF) band (30–300 GHz spectrum) or mmWave band share similar propagation characteristics, therefore, referred to as the mmWave band [5], [6].

The introduction of mmWave technology as a key player for the 5G wireless broadband communication has enabled provision of multi-gigabit communication services, such as device-to-device communication (D2D) [5]–[8], high definition television (HDTV) and ultra-high definition video (UHDV) [5], [6] and [9]–[11].

The existing and ongoing campaign efforts targeting 5G channel measurement and modeling on the 20 GHz to 30 GHz and 50 GHz to 70 GHz ranges have been reported by organizations such as New York University (NYU) and the Mobile and wireless community Enablers for the Twenty-Twenty Information Society (METIS) [4], [12]. However, a few report on the 10 GHz to 25 GHz and 40 GHz to 55 GHz bands. Accordingly, these frequency bands will require study in the future [13]. This work has been limited by channel sounder specifications to 14 GHz to 22 GHz frequency bands.

Path loss models for indoor mmWave propagation channels are important components for the design, planning, performance evaluation and deployment of wireless networks. Consequently, several organizations [14]–[16] are currently participating in developing mmWave channel models. Path

loss dictates the signal-to-noise plus interference ratio and data rates, hence network coverage area. Moreover, mmWave system simulations require accurate path loss models because it is a central parameter in wireless propagation channel [17]. A number of empirical-statistical path loss models proposed in prior research were based on linear regression to measurements such as the Okumura–Hata models [18], the COST 231 path loss models [19], and others [20]–[22].

Indoor environment is significantly different from the outdoor in many ways. As a consequence, indoor path loss models need to consider the variations in floor plans, construction materials used, type and number of office equipment, people working and their movements, scale of smart devices used in the vicinity, etc. In addition, multipath propagation along with usual fading and path loss due to distance, interference, shadowing, reflection, refraction, scattering, and penetration, also impact on the received signal characteristics [23].

In this paper, dual slope path loss model is applied. The model considers modal attenuation due to multipath and propagating wave guiding effect in indoor corridors as opposed to shadowing which has been given attention in the literature. We discuss two very important aspects of a corridor typical path loss model propagation phenomena: wave guiding effects in a corridor and break point. We have particularly conducted measurement campaigns in the 14 GHz and 22 GHz frequency bands and applied a dual slope path loss model. Break point or dual slope models have been a popular generalization for decades with determination of model parameters via a linear regression of the experimental data. Corridors are regarded as oversize dielectric waveguides with transversal dimensions much larger than wavelength, thus a number of modes are entirely involved in the propagation process. Certainly, propagating field in corridors is through superimposition of proper characteristics modes [24]–[26]. Moreover, the modal attenuation approach is mostly bounded by the fundamental mode which is least attenuated and occurs after the break point [27].

The rest of this paper is organized as follows: Detailed description of measurement equipment, hardware, environment and procedure is provided in Section II. In Section III, the analysis of large-scale path loss model, modal attenuation based dual slope model and single slope single-frequency models, propagation in indoor corridors and break point analysis are presented. In Section IV, effects of frequency, antenna height, wave guiding and construction materials are comprehensively discussed. Finally, Section V presents summarized findings of the applied dual slope model as a simple and accurate model and observed to outperform the well-known close-in reference distance model in indoor corridors at 14 GHz and 22 GHz frequency bands.

II. MEASUREMENT CAMPAIGN

In this section, we present a detailed description of the channel sounder and scenarios considered in this measurement campaign. We used Rohde and Schwarz SMF 100A for signal generation at the transmitter (Tx), Rohde and Schwarz FSIQ 40 Signal Analyzer at receiver (Rx) and two directional pyramidal horn antennas. Fig. 1 depicts the channel sounder used in our measurement campaign.

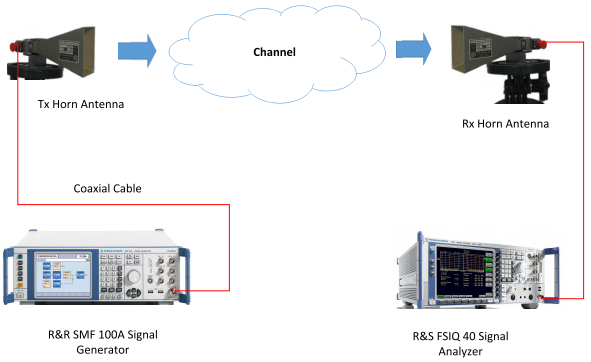

FIGURE 1. Channel sounder architecture.

TABLE 1. Channel sounder specifications and parameters configuration.

Parameter	Configuration	Units
Center Frequencies	14 and 22	GHz
Bandwidth	100	MHz
Transmission Signal	Continuous Wave	-
Tx and Rx Ant.	Direc. Horn Ant.	-
Tx Antenna Power	10	dBm
Tx Antenna Height	1.6 and 2.3	m
Rx Antenna Height	1.6	m
Tx and Rx Ant. Gain at 14 GHz	19.5	dBi
Tx and Rx Ant. Gain at 22 GHz	22.1	dBi
Tx/Rx Azm. HPBW at 14 GHz	18.4	Degrees
Tx/Rx Elev. HPBW at 14 GHz	19.2	Degrees
Tx/Rx Azm. HPBW at 22 GHz	15	Degrees
Tx/Rx Elev. HPBW at 22 GHz	13	Degrees
Tx/Rx Ant. Polarization	Vertical	-

A. MEASUREMENT EQUIPMENT AND HARDWARE

Measurements were performed with a channel sounder system based on Rohde and Schwarz SMF 100A for radio frequency signal generation at the Tx side with a frequency range of 100 kHz to 22 GHz. Rx equipment was Rohde and Schwarz FSIQ 40 Signal Analyzer with a frequency range of 20 Hz to 40 GHz and maximum analysis bandwidth of 120 MHz. Measurement system consisted of a pair of wideband directional pyramidal horn antennas with a 19.5 dBi gain, 3 dB beamwidth of 19.2° in elevation and 18.4° in azimuth and 22.1 dBi gain, 3 dB beamwidth of 13° in elevation and 15° in azimuth, at 14 GHz and 22 GHz respectively. A continuous wave was transmitted by the transmitter at 10 dBm and received power recorded at the receiver. Figs. 2 and 3 show photos of the Tx and Rx units used during measurement campaigns. Table. 1 provides the parameters configuration and equipment specifications.

B. MEASUREMENT SCENARIO AND EXPERIMENTAL PROCEDURE

We conducted measurement campaigns within the indoor corridor on 5th floor of the Discipline of Electrical, Electronic

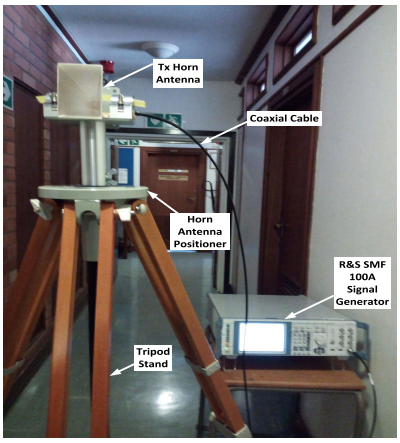

FIGURE 2. Transmitter system.

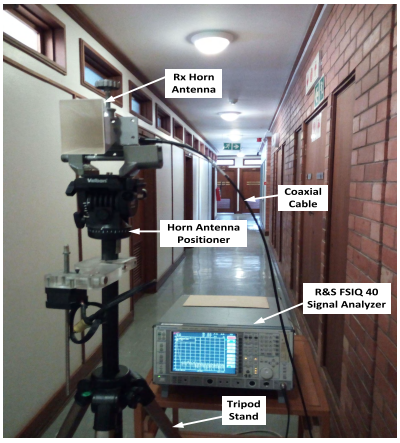

FIGURE 3. Receiver system.

FIGURE 4. Indoor corridor.

and Computer Engineering building, University of Kwa-Zulu Natal, South Africa. The measurement environment was a typical indoor corridor, a waveguide like structure with walls made of bricks and dry concrete, wooden doors to offices, a staircase and an elevator (see Fig. 4). The Tx antenna was installed at 1.6 m and 2.3 m (typical hotspot indoor location) and Rx antenna at 1.6 m (typical handset height) above the floor. With Tx antenna fixed at one end of the corridor, Rx antenna was placed at thirteen (13) different locations for both line-of-sight (LOS) and non-line-of-sight (NLOS) measurements. The directional horn antenna at the Rx side was rotated over azimuth angles with 10° azimuth steps. Measurements were performed with identical Tx and Rx locations for both 14 GHz and 22 GHz to enable direct juxtaposition between the two frequency bands. Pyramidal horn antennas with vertical polarization were used for all measurement tests.

We selected a single Tx location, with antenna installed at 1.6 m and 2.3 m high and thirteen (13) Rx identical locations for both Tx antenna heights. The Tx-Rx separation distances varied from 2 m to 24 m in steps of 2 m per measurement location. The indoor corridor dimensions were 1.4 m (wide) by 30 m (long) by 2.6 m (high). Fig. 5 displays the floor map and Tx and Rx locations. For each Tx-Rx antenna combination, the Rx was rotated in steps of 10° in the azimuth plane while elevation was fixed at 0° for both 14 GHz and 22 GHz frequency bands. The incremental rotation enabled 36 different angles of arrival (AOAs) data over 360° azimuth plane in every Rx location. Tx antenna was fixed at 0° in both elevation and azimuth at 1.6 m in height while at 2.3 m Tx high, the azimuth and elevation of the antenna were fixed at 0° and −20° respectively.

We post-processed the measurement data of received power at every point in steps of 2 m from Tx to Rx along the axial length of the corridor. Received power at every measurement point was then averaged from data set at that point. Finally, the path loss was determined by converting the power received at each point.

This measurement scenario was motivated by the need to develop a path loss model that considers multipath propagation in waveguide like structures for future networks. Consequently, an indoor corridor with bricks and dry concrete walls and ceiling, wooden doors and tiled floor was selected. A propagating signal in a corridor travels from Tx to Rx via a LOS (direct) path, and NLOS (reflected, scattered, and/or diffracted) paths, but not penetration of an obstacle. A closed-plan environment is a scenario where a propagating signal must penetrate an obstacle to get at the receiver [28], hence shadowing. However, this study focuses on an open-plan environment; an indoor corridor with modal attenuation in the application of dual slope model.

First, LOS path loss was established for scenarios where Tx and Rx had no obstruction between them and pointed at each other with alignment on boresight. Next, the NLOS path loss was established in the environment where Tx and Rx had a clear LOS path to one another, but the antennas were out of alignment on boresight. Finally, NLOS-Best path loss was established from the strongest signal power measured at NLOS environment for each exclusive antenna pointing angles in every Tx and Rx combination [28]. We analytically demonstrate the suitability of our model for various set ups in Section III.

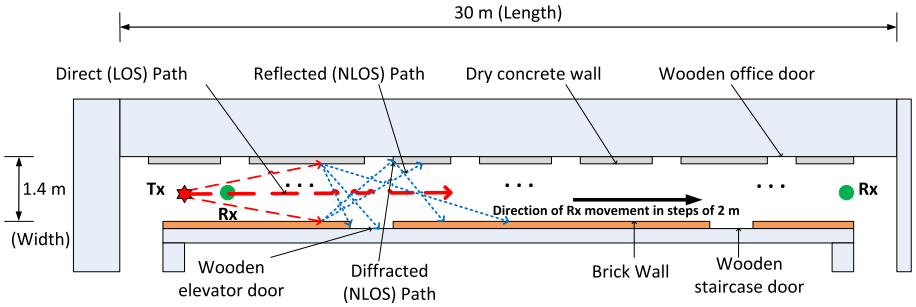

FIGURE 5. Floor plan of the indoor corridor.

III. ANALYSIS OF LARGE-SCALE PATH LOSS MODEL

Large-scale path loss models predict the propagating signals' attenuation over distance. They are important in designing a more efficient future generation communication systems. The wave guiding propagation mechanism (multipath) in corridors necessitates the wave to propagate from Tx to Rx in such scenarios. It is important to establish the dominant propagation mechanisms in indoor corridors in order to model path loss for 5th generation networks. In this paper, we consider the dominant propagation paths in modeling large-scale path loss in indoor corridor environments.

Complexity of indoor environments generate strong multipath propagation- reflections, diffractions, penetration and shadowing effects that have significant impact on received power [29]. Due to the multiple reflections and wave guiding effects, the signal power at a receiving point is expressed as a sum of direct and reflected paths from the source. Incidentally, both mode conversion and propagation losses increase due to imperfectness of the waveguide such as the sidewall roughness, tilt, obstacles, etc. [27], [30], and [31]. We analyse the impact of mode attenuation on path loss in a rectangular indoor corridor in Section III-A.

This paper considers signal attenuation as it bounces on the corridor walls, floor and ceiling. We assume that the wave propagates mostly in longitudinal direction inside the corridor and effects of wooden doors and losses due to roughness of sidewalls and tilt are small.

A. WAVEGUIDE BASED CHANNEL MODEL

Based on the geometry and conductivity of construction materials in a tunnel, just like a corridor, radio propagation can be modeled in the same way as radio waves in a waveguide. The guiding wave phenomenon emerges at frequencies of a few hundred MHz and above [25], [27]. Prior research has shown, however, that the wave guiding effect occurs only in tunnels with larger transverse dimensions than wavelength of the signal [32]–[34].

The radio signal attenuation in waveguides (e.g tunnels and corridors) is usually much lower than in free space and decreases with increasing frequency due to wave guiding effect. Therefore, at mmWave, imperfections in the conducting walls of the corridor mainly cause path losses thus modeled as a waveguide [34], [35].

The possible modes in a rectangular waveguide i.e (m,n) modes can be geometrically described as a cluster of propagating wave into the corridor reflected on the vertical and horizontal walls with proper grazing angles $\phi_V^{m,n}$ and $\phi_H^{m,n}$ respectively. The electromagnetic field produced by these waves propagate progressively along the corridor's axis and on the contrary a full standing wave in the xy plane, where the waves superimpose to produce the (m,n) mode behavior [24]. The grazing angles can be derived by the following relations:

$$sin\phi_H^{m,n} = \frac{\lambda \cdot n}{2h} \tag{1}$$

$$sin\phi_V^{m,n} = \frac{\lambda \cdot m}{2w} \tag{2}$$

where λ is the wavelength, h is the height while w is the width of the corridor, n and m are x and y polarized mode numbers respectively.

From the mode geometrical description in (1) and (2), analytical expressions of distance between two consecutive bounces on the vertical $\Delta_V^{m,n}$ and horizontal $\Delta_H^{m,n}$ walls associated with the (m,n) modes can be realized by means of trigonometrical considerations as:

$$\Delta_V^{m,n} = \frac{w}{tan(\phi_V^{m,n})} \cdot \sqrt{1 - \frac{sin^2(\phi_H^{m,n})}{cos^2(\phi_V^{m,n})}} \tag{3}$$

$$\Delta_H^{m,n} = \frac{h}{tan(\phi_V^{m,n})} \cdot \sqrt{1 - \frac{sin^2(\phi_V^{m,n})}{cos^2(\phi_H^{m,n})}} \tag{4}$$

The most likely radiators to be used in future networks are directional antennas pointed in the corridor's axis direction. Consequently, the strong waves transmitted by the Tx antenna will impinge on the corridor walls with fairly small grazing angles. The corresponding modes can be expected to have the largest amplitudes. Therefore, modes with high grazing angle values can be considered negligible, thus (3) and (4) can be simplified as (5) and (6) respectively. In addition, the number of reflections on the vertical wall ($N_V^{m,n}$) and horizontal wall ($N_H^{m,n}$) given as (7) and (8) respectively.

$$\Delta_V^{m,n} = \frac{w}{tan(\phi_V^{m,n})} \cdot cos\phi_H^{m,n} \tag{5}$$

$$\Delta_H^{m,n} = \frac{h}{tan(\phi_H^{m,n})} \cdot cos\phi_V^{m,n} \tag{6}$$

$$N_V^{m,n} = \frac{d}{\Delta_V^{m,n}} \tag{7}$$

$$N_H^{m,n} = \frac{d}{\Delta_H^{m,n}} \tag{8}$$

Finally, from (5)–(8), the *modal attenuation factor* (MAF) value, denoted by $L_{m,n}[dB]$, is given in (9). MAF is the power loss due to the multiple reflections on the mode wavefronts on the corridor walls. It is expressed as:

$$\begin{aligned} L_{m,n}[dB] &= 10\Bigg(N_V^{m,n} \cdot log_{10}\frac{1}{|R_V(\phi_V^{m,n})|^2} \\ &\quad + N_H^{m,n} \cdot log_{10}\frac{1}{|R_H(\phi_H^{m,n})|^2}\Bigg) \\ &= 10d\Bigg(\frac{tan(\phi_V^{m,n})}{w \cdot cos(\phi_H^{m,n})} \cdot log_{10}\frac{1}{|R_V(\phi_V^{m,n})|^2} \\ &\quad + \frac{tan(\phi_H^{m,n})}{h \cdot cos(\phi_V^{m,n})} \cdot log_{10}\frac{1}{|R_H(\phi_H^{m,n})|^2}\Bigg) \end{aligned} \tag{9}$$

where R_V and R_H are the reflection coefficients of the vertical and horizontal walls respectively. We approximated the reflection coefficients in this paper as follows: floor (tile) as 0.1574, wall (brick) as 0.2037, wall and ceiling (dry concrete) as 0.3112 [36].

B. SINGE SLOPE CLOSE-IN REFERENCE MODEL

Single-slope close-in reference distance (CI) path loss model can be expressed as:

$$PL^{CI}(d)[dB] = PL_{FS}(d_\circ) + 10 \times n_1 \times log_{10}\left(\frac{d}{d_o}\right) + X_\sigma^{CI} \quad for\ d \le d_\circ,\ d_\circ = 1m \tag{10}$$

where X_σ^{CI} is a zero mean Gaussian random variable with standard deviation σ in dB. $PL_{FS}(d_\circ) = 10log_{10}\left(\frac{4\pi d_\circ}{\lambda}\right)$ at physically based reference distance $d_\circ$. The path loss model is found by determination of path loss exponent (PLE) n_1 via minimum mean square error method [28].

C. PROPOSED DUAL SLOPE MODEL

Expression for proposed path loss can be written as:

$$PL^p(d)[dB] = \begin{cases} PL_1^p(d)[dB], & \text{for } d \le d_{break} \\ PL_2^p(d)[dB], & \text{for } d \ge d_{break} \end{cases} \tag{11}$$

where

$$PL_1^p(d)[dB] = PL_{FS}(d_o) + 10 \times n_1 \times log_{10}\left(\frac{d}{d_o}\right) + L_{m,n_1}(d),$$

$$PL_2^p(d)[dB] = PL_{break} + 10 \times n_2 \times log_{10}\left(\frac{d}{d_{break}}\right) + L_{m,n_2}(d)$$

and

$$PL_{break}[dB] = PL_{FS}(d_o) + 10 \times n_1 \times log_{10}\left(\frac{d_{break}}{d_o}\right)$$

Therefore

$$PL^p(d)[dB] = PL_1^p(d)[dB] + PL_2^p(d)[dB] + X_\sigma^p \quad for\ d \ge d_\circ,\ d_\circ = 1m \tag{12}$$

where $PL^p(d)[dB]$ is the path loss at any distance d between Tx and Rx, $PL_1^p(d)[dB]$ and $PL_2^p(d)[dB]$ are the path losses before and after break point respectively, d_{break} is the break point while $PL_{break}[dB]$ is the path loss at break point. Additionally, X_σ^p is a zero mean Gaussian random variable with standard deviation σ in dB, $L_{m,n_1}(d)$ and $L_{m,n_2}(d)$ are modal attenuations before and after the break point respectively.

It follows that dual slope path loss model is found by determination of the path loss exponent (PLE) n_1 (before break point) and n_2 (after break point)via the minimum mean square error method.

Generally, a large number of path models presented in a dual slope curve to describe the propagation inside tunnels and indoor corridor. They are described by two different expressions [25]. A break point (dividing point) between two slopes separates the models into two segments [37]. There were no waveguide effects experienced before the break point, where the high order modes are dominant; hence, the propagating signal suffered a stronger path loss and fluctuation. However, after the break point, the propagating wave suffers smaller loss and slight fading as the fundamental modes guide the propagation in the corridor [38]. In Section III-D, a detailed explanation of extra path loss due to modal attenuation is presented.

D. EXTRA PATH LOSS

The elemental aspect inherent in radio wave propagation is wavefront divergence. Wavefront is the edge of a propagating wave. As the wavefront propagates spherically, its surface enlarges, consequently, its power density decreases with the square of the distance. This decrease accordingly satisfies power-flux conservation. Apart from free-space propagation, (10) in principle may also describe propagation in guiding structures. In such structures, a quasi-2-D propagation with wave divergence proportional to the first power of distance should take place. However, the presence of material losses usually results in higher values with respect to the ideal cases [24], [39].

Path loss models are normally based on measurement campaigns such as [4], [40], and [41] or ray tracing [42], [43]. Most path loss models assume a simple power-law dependence on distance using a logarithmic scale (10) which is a straight line in a $'log-log'$ plot. However, the proposed model is a dual slope path loss on a linear scale.

Equation (10), however, cannot properly account for waveguide effects in corridor, which often occur in indoor propagation due to structural position of walls, floor and ceilings. This scenario results in a site-specific linear excess path loss term $L_{m,n}[dB]$ (see (9)). We modeled this excess attenuation term through a linear instead of algorithmic form. We apply a dual slope path loss model (see, (11)) as a

TABLE 2. Regression analysis of single frequency directional large-scale path loss for 14 GHz and 22 GHz with Rx antenna height fixed at 1.6 m and Tx antenna height at 1.6 m and 2.3 m above the ground.

Freq	Tx Height (m)	Rx Height (m)	Path Loss Model	LOS			NLOS-Best			NLOS		
				PLE		σ[dB]	PLE		σ[dB]	PLE		σ[dB]
				n_1	n_2		n_1	n_2		n_1	n_2	
14 GHz	1.6	1.6	Close-In Ref.	1.7	-	2.5	1.9	-	4.9	2.1	-	5.2
			Proposed	1.7	0.1	2.2	1.9	0.1	3.5	2.1	0.1	3.7
	2.3	1.6	Close-In Ref.	1.6	-	4.0	1.9	-	6.1	2.0	-	6.2
			Proposed	1.6	0.5	3.9	1.9	0.1	5.0	2.0	0.1	5.1
22 GHz	1.6	1.6	Close-In Ref.	1.6	-	1.3	1.7	-	4.6	1.9	-	5.2
			Proposed	1.6	0.1	1.1	1.7	0.1	3.5	1.9	0.1	3.8
	2.3	1.6	Close-In Ref.	1.7	-	4.8	1.7	-	5.4	2.0	-	6.4
			Proposed	1.7	0.1	4.3	1.7	0.1	4.3	2.0	0.2	5.0

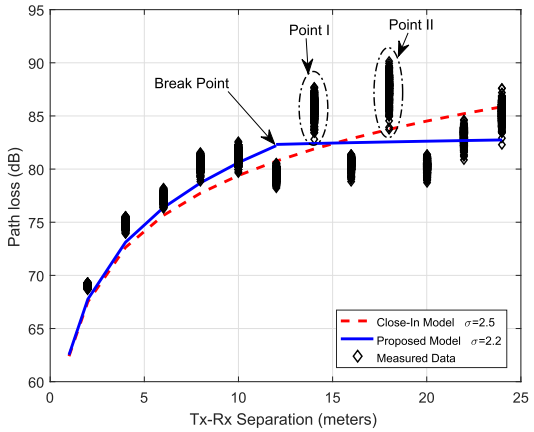

FIGURE 6. 14 GHz directional LOS large-scale path loss with Tx antenna: 1.6 m and Rx antenna: 1.6 m.

combination of (9) and (10). This dual slope path loss model accounts for multipath propagation mechanisms in a corridor. Finally, this model is simple and accurate, hence suitable for general design and planning of network deployment in indoor environments.

E. BREAK POINT

As highlighted in Section III-C, it is critical to establish how the different propagation mechanisms in corridors give rise to multipath. In this context, it is worthwile to note that diffraction plays a lesser role in the mmWave regime. Consequently, in NLOS scenario, the receiver will rely instead on ambient reflected paths [44]–[46]. We determined the break point using measurement data. We established the break point (see Fig. 6) in this work at approximately 12 m from Tx and expressed by (13):

$$d_{break} = \sqrt{\frac{a^2}{\lambda}} \tag{13}$$

where a is the maximum dimension of a corridor and λ is the signal wavelength. Accordingly, path loss increases linearly from $d = 1$ to d_{break}, further, it increases with a different linear slope there after (12).

IV. DISCUSSION

Unambiguous understanding of propagation mechanisms in an indoor environment is imperative for accurate path loss channel modeling in mmWave communication systems. In this section, we discuss the impacts of direct transmitted, reflected and diffracted paths on path loss in indoor corridors with regards to transmission frequency and antenna height.

A. FREQUENCY OF TRANSMISSION

We conducted measurement campaign at 14 GHz and 22 GHz to establish a more accurate and meaningful path loss model for propagation in indoor corridors. The LOS, NLOS-Best and NLOS paths provided a much broader analysis of propagation in a corridor. First, we analyzed experimental data of thirteen (13) Rx locations, 36 azimuth orientations per Rx location for 2 different Tx heights at each of the frequency bands. The applied dual slope path loss model considered the modal attenuation of multipath and out performs the close-in reference distance model in all the scenarios and frequency bands. Regression analysis presented in Table 2. Close-in reference distance model has a single PLE (n_1) while dual slope model has two (n_1 and n_2, Table 2). Comparatively, the standard deviation σ of the signal fluctuation of dual slope model around the mean path loss was lower than close-in reference model, hence more accurate in predicting path loss as provided in Table 2. Direct LOS path from Tx to Rx is illustrated by red dashed arrow, reflected and diffracted paths from corridor walls (reflected paths from ceiling and floor are not shown) and knife-edge doors by blue dot line respectively as shown in Fig. 5.

Figure 6 illustrates the analysis of LOS dual slope path loss model fitting on measurement data. Before the point, wave propagation comprises of free space and multi-mode waveguide mechanisms. Subsequently, high order modes are dominant and wave guiding is effect not established. However, after the break point, the wave undergoes relatively low loss and negligible fading as high-order modes much attenuated and the fundamental modes guide the propagation [38].

The multipaths had insignificant effect on path loss as high order modes were greatly attenuated before break point at both 14 GHz and 22 GHz bands. However, after break

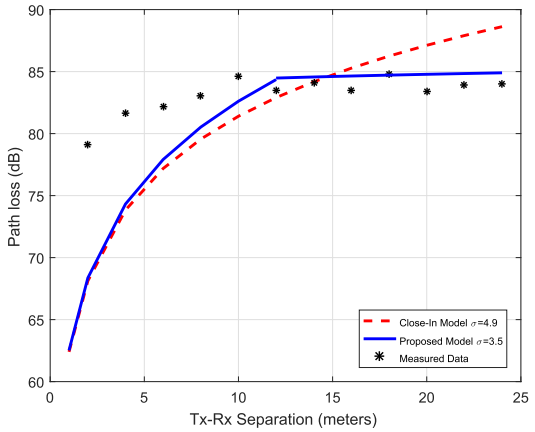

FIGURE 7. 14 GHz directional NLOS-Best large-scale path loss with Tx antenna height: 1.6 m and Rx antenna: 1.6 m.

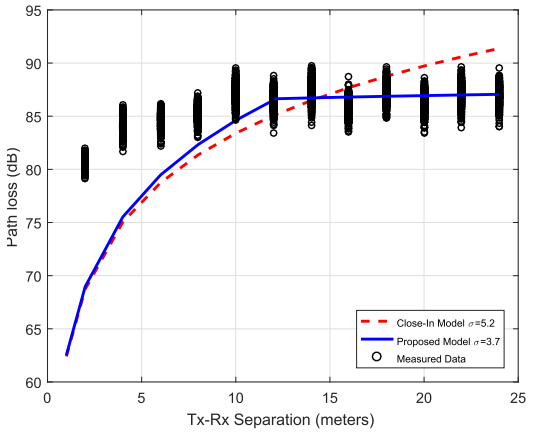

FIGURE 8. 14 GHz directional NLOS large-scale path loss with Tx antenna: 1.6 m and Rx antenna: 1.6 m.

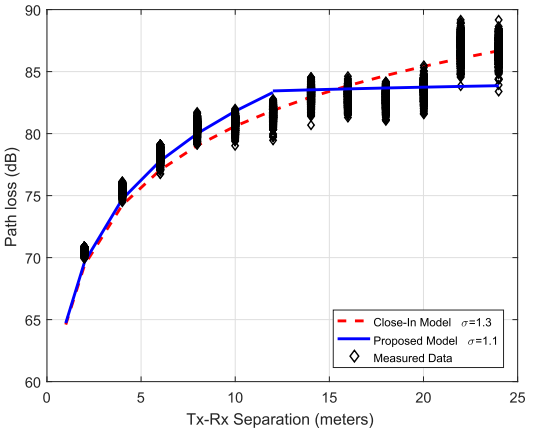

FIGURE 9. 14 GHz directional LOS large-scale path loss with Tx antenna: 2.3 m and Rx antenna: 1.6 m.

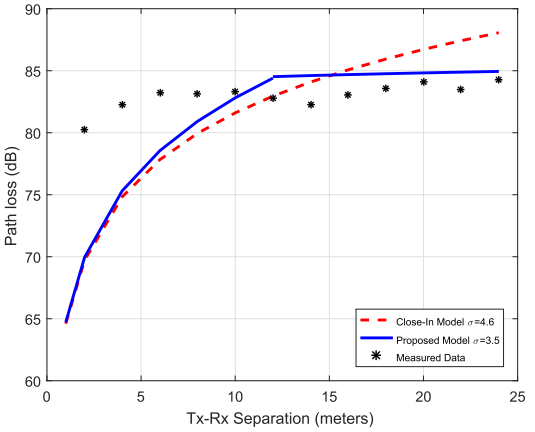

FIGURE 10. 14 GHz directional NLOS-Best large-scale path loss with Tx antenna: 2.3 m and Rx antenna height: 1.6 m.

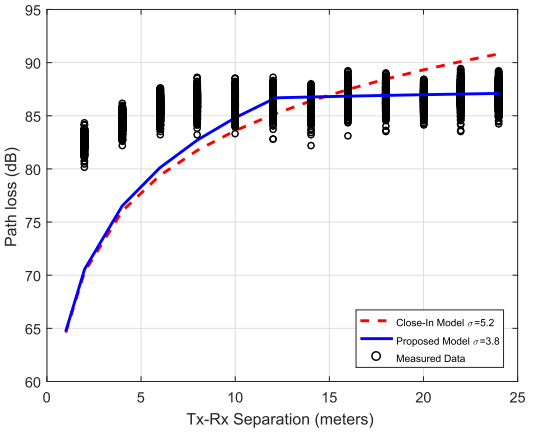

FIGURE 11. 14 GHz directional NLOS large-scale path loss with Tx antenna: 2.3 m and Rx antenna: 1.6 m.

point, destructive and constructive interference attributed to multipaths on LOS direct path were observed (Point I and II) at both antenna heights as shown in Figs. 6, 9, 12 and 15. Undoubtedly, due to multipath existence, signals on NLOS and NLOS-Best environments were recorded. However, little reflections and diffractions were experienced between 2 m and 4 m from the Tx due to directivity of the transmission as shown in Figs. 7, 8, 10, and 11 and Figs. 13, 14, 16, 17 for 14 GHz and 22 GHz respectively. Furthermore, after 4 m away from Tx, Fig. 5, the received signal power was predominantly as a result of reflected and diffracted paths. Finally, the guided wave thereafter maintained the signal strength through the corridor, hence slow increase in path loss. As expected, the radio signal attenuation decreased with increasing frequency due to wave guiding effect.

B. ANTENNA HEIGHT

A summarized analysis of large-scale parameters is presented in Table 2 for Tx height: 1.6 m and 2.3 m. The Rx height was maintained at 1.6 m for all measurement points. First, we conducted measurements with Tx height at 1.6 m for 14 GHz and 22 GHz bands. PLE (n_1) decreased for LOS and NLOS with increase in Tx height. In addition, it can be seen from Table 2 that signal is better confined in a corridor as it propagates at higher antenna heights. Typically, Tx antennas in indoor environments are installed at about 2.6 m above the floor. However, NLOS-Best PLE (n_1) remained constant

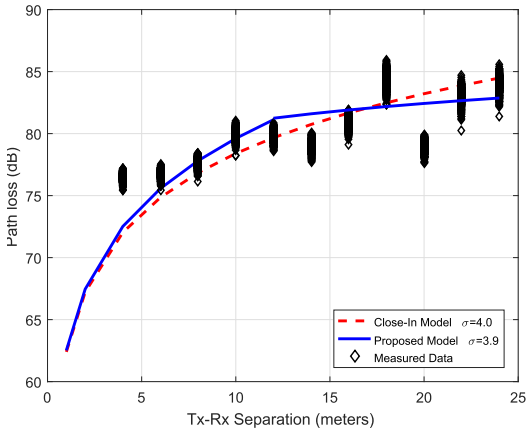

FIGURE 12. 22 GHz directional LOS large-scale path loss with Tx antenna: 1.6 m and Rx antenna: 1.6 m.

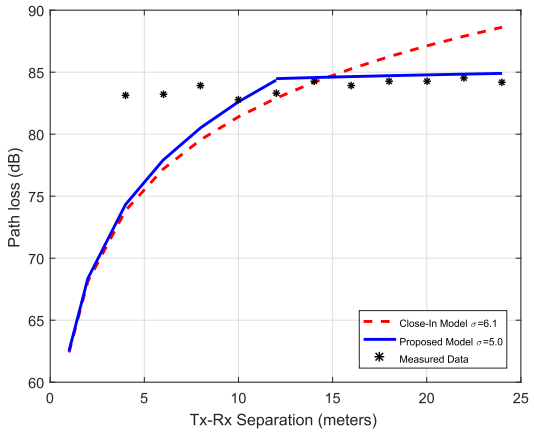

FIGURE 13. 22 GHz directional NLOS-Best large-scale path loss with Tx antenna: 1.6 m and Rx antenna: 1.6 m.

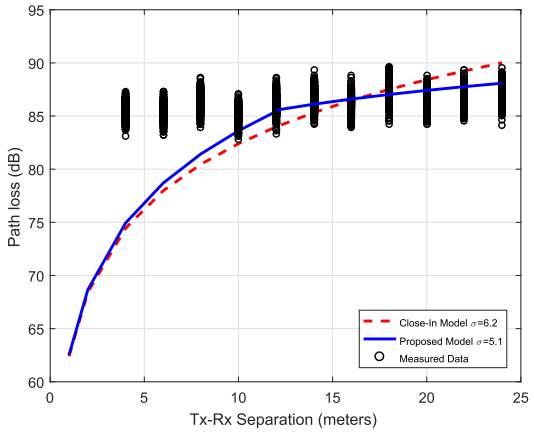

FIGURE 14. 22 GHz directional NLOS large-scale path loss with Tx antenna: 1.6 m and Rx antenna: 1.6 m.

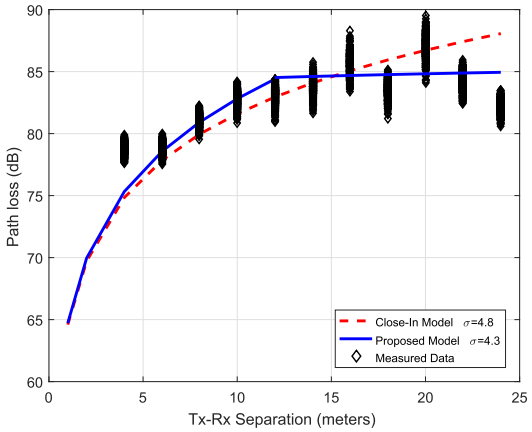

FIGURE 15. 22 GHz directional LOS large-scale path loss with Tx antenna: 2.3 m and Rx antenna: 1.6 m.

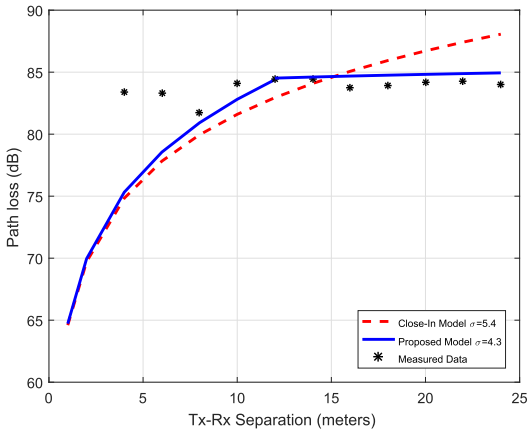

FIGURE 16. 22 GHz directional NLOS-Best large-scale path loss with Tx antenna: 2.3 m and Rx antenna: 1.6 m.

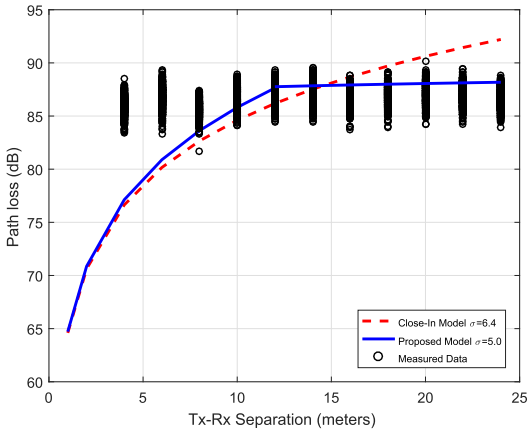

FIGURE 17. 22 GHz directional NLOS large-scale path loss with Tx antenna: 2.3 m and Rx antenna: 1.6 m.

at both Tx heights. Second, with transmission frequency set at 22 GHz and Tx height at 1.6 m and 2.3 m, in contrast, LOS and NLOS PLE (n_1) decreased apparently because of more destructive interference at higher frequencies from the reflected waves in the corridor as shown in Figs. 15 and 17. Finally, stronger constructive interferences and better wave guiding effect in the corridor were experienced with increase in Tx height from 1.6 m to 2.3 m and LOS PLE (n_1) decreased from 1.7 to 1.6 at 14 GHz. As the frequency increases, signal attenuation decreases in a waveguide [35].

V. CONCLUSION

The main objective of this work was to establish a simple and accurate path loss model for indoor corridor for future networks. A dual slope path loss model is proposed that accounts for major propagation mechanisms in indoor environments. Generally, corridors confine propagating wave as indicated by PLE less than that of free space (typically 2) in indoor measurement scenarios (Table 2) and supported by literature [28] and [44]. Major portion of the path loss occur before break point as the propagation mechanisms are free space and multi-modal. However, after the break point, the guiding effect of the corridor begins. Consequently, a signal is confined as it propagates in the corridor hence a dual slope path loss model applies.

Building materials and structural design of buildings call for development of site-specific path loss models. Equally, both antenna height and the frequency of propagation do play an important role in indoor path loss modeling. This proposed model is observed to outperform the close-in reference model in all measurement conditions. Certainly, an accurate path loss model is essential for design and deployment of future communication systems. Finally, an investigation of the constructive and destructive interference is fundamental for deeper understanding of the propagation mechanisms specifically in indoor corridors.

ACKNOWLEDGMENT

The authors would like to acknowledge the support and participation of the following postgraduate students during measurement campaign: O. Kolawole, F. Chelangat and E. Kataka.

REFERENCES

[1] A. M. Al-Samman, T. A. Rahman, M. H. Azmi, M. N. Hindia, I. Khan, and E. Hanafi, "Statistical modelling and characterization of experimental mm-wave indoor channels for future 5G wireless communication networks," *PLoS ONE*, vol. 11, no. 9, pp. 1–29, Sep. 2016.

[2] S. Chitra and N. Kumaratharan, "Intercarrier interference reduction in MC-CDMA system through second order duobinary coded phase rotated conjugate cancellation scheme," *PLoS ONE*, vol. 10, no. 3, pp. 1–14, Mar. 2015.

[3] M. N. Hindia, A. W. Reza, K. A. Noordin, and M. H. R. Chayon, "A novel LTE scheduling algorithm for green technology in smart grid," *PLoS ONE*, vol. 10, no. 4, pp. 1–18, Apr. 2015.

[4] T. S. Rappaport *et al.*, "Millimeter wave mobile communications for 5G cellular: It will work!" *IEEE Access*, vol. 1, pp. 335–349, May 2013.

[5] Z. Pi and F. Khan, "An introduction to millimeter-wave mobile broadband systems," *IEEE Commun. Mag.*, vol. 49, no. 6, pp. 101–107, Jun. 2011.

[6] T. S. Rappaport, G. R. MacCartney, M. K. Samimi, and S. Sun, "Wideband millimeter-wave propagation measurements and channel models for future wireless communication system design," *IEEE Trans. Commun.*, vol. 63, no. 9, pp. 3029–3056, Sep. 2015.

[7] Q. Du, H. Song, Q. Xu, P. Ren, and L. Sun, "Interference-controlled D2D routing aided by knowledge extraction at cellular infrastructure towards ubiquitous CPS," *Pers. Ubiquitous Comput.*, vol. 19, no. 7, pp. 1033–1043, Oct. 2015.

[8] H. He, Q. Du, H. Song, W. Li, Y. Wang, and P. Ren, "Traffic-aware ACB scheme for massive access in machine-to-machine networks," in *Proc. IEEE Int. Conf. Commun. (ICC)*, Jun. 2015, pp. 617–622.

[9] H. A. Syed, H. B. Safdar, and S. Houbing, "Multimedia streaming in named data networks and 5G networks," *IEEE COMSOC MMTC E-Lett.*, vol. 11, no. 2, pp. 57–61, Mar. 2016.

[10] M. Elkashlan, T. Q. Duong, and H.-H. Chen, "Millimeter-wave communications for 5G: Fundamentals: Part I [guest editorial]," *IEEE Commun. Mag.*, vol. 52, no. 9, pp. 52–54, Sep. 2014.

[11] D. Liu *et al.*, "User association in 5G networks: A survey and an outlook," *IEEE Commun. Surveys Tuts.*, vol. 18, no. 2, pp. 1010–1044, 2nd Quart., 2016.

[12] *METIS Deliverable D1.4, METIS Channel Models*, Mobile Wireless Commun. Enablers Twenty-Twenty Inf. Soc., Stockholm, Sweden, Feb. 2015.

[13] T. Imai, K. Kitao, N. Tran, and N. Omaki, "Radio propagation for 5G," *NTT DOCOMO Tech. J.*, vol. 17, no. 4, pp. 40–49, Apr. 2016.

[14] *Channel Modeling for Higher Frequency Bands*, document RP 151306, 3GPP, Jun. 2015.

[15] *5G Millimeter Wave Channel Model Alliance*. Accessed: Nov. 5, 2017. [Online]. Available: http://www.nist.gov/ctl/upload/5G-Millimeter-Wave-Channel-Model-AllianceV2.pdf

[16] *METIS Deliverables D1.2, Initial Channel Models Based on Measurements*. Accessed: Nov. 5, 2017. [Online]. Available: https://www.metis2020.

[17] A. F. Molisch, *Wireless Communications*, 2nd ed. Hoboken, NJ, USA: Wiley, 2011.

[18] Y. Okumura, E. Ohmori, T. Kawano, and K. Fukuda, "Field strength and its variability in VHF and UHF land-mobile radio service," *Rev. Elect. Commun. Lab.*, vol. 16, nos. 9–10, pp. 825–873, 1968.

[19] E. Damosso and L. M. Correia, "COST action 231: Digital mobile radio towards future generation systems," Eur. Commission, Brussels, Belgium, Tech. Rep. 18957, 1999.

[20] C. Phillips, D. Sicker, and D. Grunwald, "A survey of wireless path loss prediction and coverage mapping methods," *IEEE Commun. Surveys Tuts.*, vol. 15, no. 1, pp. 255–270, 1st Quart., 2013.

[21] K. Haneda, "Channel models and beamforming at millimeter-wave frequency bands," *IEICE Trans. Commun.*, vol. E98.B, no. 5, pp. 755–772, May 2015.

[22] A. F. Molisch *et al.*, "Millimeter-wave channels in urban environments," presented at the 10th Eur. Conf. Antennas Propag. (EuCAP), Davos, Switzerland, Apr. 2016.

[23] H. K. Rath, S. Timmadasari, B. Panigrahi, and A. Simha, "Realistic indoor path loss modeling for regular WiFi operations in India," in *Proc. 23rd Nat. Conf. Commun. (NCC)*, vol. 1. Mar. 2017, pp. 1–6.

[24] F. Fuschini and G. Falciasecca, "A mixed rays—Modes approach to the propagation in real road and railway tunnels," *IEEE Trans. Antennas Propag.*, vol. 60, no. 2, pp. 1095–1105, Feb. 2012.

[25] D. G. Dudley, M. Lienard, S. F. Mahmoud, and P. Degauque, "Wireless propagation in tunnels," *IEEE Antennas Propag. Mag.*, vol. 49, no. 2, pp. 11–26, Apr. 2007.

[26] Z. Sun and I. F. Akyildiz, "Channel modeling and analysis for wireless networks in underground mines and road tunnels," *IEEE Trans. Commun.*, vol. 58, no. 6, pp. 1758–1768, Jun. 2010.

[27] A. Emslie, R. Lagace, and P. Strong, "Theory of the propagation of UHF radio waves in coal mine tunnels," *IEEE Trans. Antennas Propag.*, vol. AP-23, no. 2, pp. 192–205, Mar. 1975.

[28] G. MacCartney, T. S. Rappaport, S. Sun, and S. Deng, "Indoor office wideband millimeter-wave propagation measurements and channel models at 28 and 73 GHz for ultra-dense 5G wireless networks," *IEEE Access*, vol. 3, pp. 2388–2424, 2015.

[29] A. Hrovat, G. Kandus, and T. Javornik, "Path loss analyses in tunnels and underground corridors," *Int. J. Commun.*, vol. 6, no. 3, pp. 136–144, Aug. 2012.

[30] Y. P. Zhang, Y. Hwang, and J. D. Parsons, "UHF radio propagation characteristics in straight open-groove structures," *IEEE Trans. Veh. Technol.*, vol. 48, no. 1, pp. 249–254, Jan. 1999.

[31] E. A. J. Marcatili and R. A. Schmeltzer, "Hollow metallic and dielectric waveguides for long distance optical transmission and lasers," *Bell Syst. Tech. J.*, vol. 43, no. 4, pp. 1783–1809, Jul. 1964.

[32] T. Klemenschits and E. Bonek, "Radio coverage of road tunnels at 900 and 1800 MHz by discrete antennas," in *Proc. 5th IEEE Int. Symp. Pers., Indoor Mobile Radio Commun. Wireless Netw.–Catching Mobile Future*, The Hague, The Netherlands, Sep. 1994, pp. 411–415.

[33] Y. P. Zhang, "Novel model for propagation loss prediction in tunnels," *IEEE Trans. Veh. Technol.*, vol. 52, no. 5, pp. 1308–1314, Sep. 2003.

[34] L. Deryck, "Natural propagation of electromagnetic waves in tunnels," *IEEE Trans. Veh. Technol.*, vol. VT-27, no. 3, pp. 145–150, Aug. 1978.

[35] A. Hrovat, G. Kandus, and T. Javornik, "A survey of radio propagation modeling for tunnels," *IEEE Commun. Surveys Tuts.*, vol. 16, no. 2, pp. 658–669, 2nd Quart., 2014.
[36] K. Sato *et al.*, "Measurements of reflection characteristics and refractive indices of interior construction materials in millimeter-wave bands," in *Proc. IEEE 45th Veh. Technol. Conf.*, vol. 1. Chicago, IL, USA, Jul. 1995, pp. 449–453, doi: 10.1109/VETEC.1995.504907.
[37] C. Briso-Rodriguez, J. M. Cruz, and J. I. Alonso, "Measurements and modeling of distributed antenna systems in railway tunnels," *IEEE Trans. Veh. Technol.*, vol. 56, no. 5, pp. 2870–2879, Sep. 2007.
[38] K. Guan *et al.*, "Complete propagation model structure inside tunnels," *Prog. Electromagn. Res.*, vol. 141, pp. 711–726, Aug. 2013, doi: 10.2528/PIER13052212.
[39] V. Degli-Esposti, G. Falciasecca, F. Fuschini, and E. M. Vitucci, "A meaningful indoor path-loss formula," *IEEE Antennas Wireless Propag. Lett.*, vol. 12, pp. 872–875, 2013, doi: 10.1109/LAWP.2013.2271532.
[40] A. Karttunen *et al.*, "Path loss models with distance-dependent weighted fitting and estimation of censored path loss data," *IET Microw., Antennas Propag.*, vol. 10, no. 14, pp. 1467–1474, Sep. 2016.
[41] S. Hur *et al.*, "Wideband spatial channel model in an urban cellular environments at 28 GHz," in *Proc. 9th Eur. Conf. Antennas Propag. (EuCAP)*, Lisbon, Portugal, Apr. 2015, pp. 1–5.
[42] S. G. Larew, T. A. Thomas, M. Cudak, and A. Ghosh, "Air interface design and ray tracing study for 5G millimeter wave communications," in *Proc. IEEE Globecom Workshops (GC Wkshps)*, Dec. 2013, pp. 117–122, doi: 10.1109/GLOCOMW.2013.6824972.
[43] V. Degli-Esposti *et al.*, "Ray-tracing-based MM-wave beamforming assessment," *IEEE Access*, vol. 2, pp. 1314–1325, 2014, doi: 10.1109/ACCESS.2014.2365991.
[44] J. Senic, C. Gentile, P. B. Papazian, K. A. Remley, and J.-K. Choi, "Analysis of E-band path loss and propagation mechanisms in the indoor environment," *IEEE Trans. Antennas Propag.*, vol. 65, no. 12, pp. 6562–6573, Dec. 2017, doi: 10.1109/TAP.2017.2722876.
[45] T. S. Rappaport, R. W. Heath, Jr., R. C. Daniels, and J. N. Murdock, *Millimeter Wave Wireless Communications*. Englewood Cliffs, NJ, USA: Prentice-Hall, 2015.
[46] S. Deng, G. R. MacCartney, and T. S. Rappaport, "Indoor and outdoor 5G diffraction measurements and models at 10, 20, and 26 GHz," in *Proc. IEEE Global Commun. Conf.*, Dec. 2016, pp. 1–7, doi: 10.1109/GLOCOM.2016.7841898.

NICHOLAS O. OYIE received the B.Tech. degree (Hons.) in electrical and communication engineering from the Masinde Muliro University of Science and Technology, Kenya, in 2009, and the M.Sc. in telecommunication engineering from the Jomo Kenyatta University of Agriculture and Technology, Kenya, in 2016. He is currently pursuing the Ph.D. degree in electronic engineering with the University of KwaZulu-Natal, Durban, South Africa, under the supervision of Prof. T. J. O. Afullo.

He was with Essar Telecom, Kenya, as a Telecommunication Engineer from 2009 to 2010. His research areas of interest include radio wave propagation, radio resource and mobility management in wireless networks, femtocells and quality of service support.

THOMAS J. O. AFULLO received the B.Sc. degree (Hons.) in electrical engineering from the University of Nairobi in 1979, the M.Sc. degree in electrical engineering from the University of West Virginia, USA, in 1983, and the Ph.D. degree in electrical engineering from Vrije Universiteit Brussel, Belgium, in 1989. He is currently a Professor with the Discipline of Electrical, Electronic and Computer Engineering, University of KwaZulu-Natal, Durban, South Africa, and a former Academic Leader.

He was with Kenya Post and Telecommunication Corporation as a Senior Executive Engineer from1985 to 1986. He was a Senior Lecturer and the Head of the Department of Electrical and Communication Engineering, Moi University, Kenya from 1991 to 1994. He was a Lecturer with the University of Botswana from 1996 to2002, an Associate Professor with UDW/UKZN from 2003 to 2010, and has been a Professor with UKZN, since 2012. His research interests include radio wave propagation, antenna design, cognitive radio, and power line communication.